Nonlinear resonances and antiresonances of a forced sonic vacuum

D. Pozharskiy, Y. Zhang, M. O. Williams, D. M. McFarland, P. G. Kevrekidis, A. F. Vakakis, and I. G. Kevrekidis

Phys. Rev. E **92**, 063203 — Published 23 December 2015

DOI: 10.1103/PhysRevE.92.063203

Nonlinear Resonances and Antiresonances of a Forced Sonic Vacuum

D. Pozharskiy,[1] Y. Zhang,[2] M.O. Williams,[1] D.M. McFarland,[3]
P.G. Kevrekidis,[4,5] A.F. Vakakis,[2] and I.G. Kevrekidis[1]

[1]*Department of Chemical and Biological Engineering and PACM, Princeton University, Princeton, NJ 08544, USA*
[2]*Department of Mechanical Science and Engineering, University of Illinois at Urbana-Champaign, 1206 West Green Street, Urbana, IL 61822, USA*
[3]*Department of Aerospace Engineering, University of Illinois at Urbana - Champaign, Urbana, IL 61822, USA*
[4]*Department of Mathematics and Statistics, University of Massachusetts, Amherst, MA 01003-4515, USA*
[5]*Center for Nonlinear Studies and Theoretical Division, Los Alamos National Laboratory, Los Alamos, NM 87544, USA*

(Dated: November 23, 2015)

We consider a harmonically driven acoustic medium in the form of a (finite length) highly nonlinear granular crystal with an amplitude and frequency dependent boundary drive. Despite the absence of a linear spectrum in the system, we identify resonant periodic propagation whereby the crystal responds at *integer multiples* of the drive period, and observe that this can lead to local maxima of transmitted force at its fixed boundary. In addition, we identify and discuss minima of the transmitted force ("antiresonances") in between these resonances. Representative one-parameter complex bifurcation diagrams involve period doublings, Neimark-Sacker bifurcations as well as multiple isolas (e.g. of period-3, -4 or -5 solutions entrained by the forcing). We combine them in a more detailed, two-parameter bifurcation diagram describing the stability of such responses to both frequency and amplitude variations of the drive. This picture supports a notion of a (purely) "nonlinear spectrum" in a system which allows no sound wave propagation (due to zero sound speed: the so-called sonic vacuum). We rationalize this behavior in terms of purely nonlinear building blocks: apparent traveling and standing nonlinear waves.

PACS numbers: 45.70.-n 05.45.-a 46.40.Cd

Introduction. In media that bear a crystalline lattice structure (perfect or imperfect), an understanding of the underlying linear spectrum is of paramount importance both for their linear wave transmission properties [1] and for the emergence of anharmonicity-induced excitations such as discrete breathers [2]. However, in recent years there has been an increased interest in systems that *do not possess a linear spectrum*. This stems to a considerable degree from the interest in discretizing prototypical nonlinear systems such as the Burgers equation [3], but also from the intrinsic mathematical (and potentially physical) interest in exploring systems with purely nonlinear dispersion; a remarkable feature of the latter has been the identification of discrete analogues of compactons [4] and of compactly supported breathers [5]. A fundamental question that then emerges in the latter context is whether an analogue of acoustic transmission/spectral features exists in these highly (or purely) nonlinear systems.

Importantly, the last two decades have also brought forth a remarkably accessible (theoretically, numerically and experimentally) example of a (tunably) highly nonlinear system. This is in the form of granular crystals, consisting of lattices of beads interacting (chiefly) elastically, by means of the so-called Hertzian contact forces [6, 7] $F = A\delta^p$. Here A is an elasticity and geometry dependent prefactor, δ is the compression-induced displacement and p the nonlinear force exponent, typically equal to 3/2. These acoustic systems enjoy a remarkable degree of tunability from homogeneous (same types of beads) to heterogeneous or disordered, and, importantly for our current purposes, from essentially linear to weakly or even highly or purely nonlinear [6–9]. The latter aspect is controlled by the amount of *a priori* compression (dubbed precompression δ_0) externally imposed on the beads. When this precompression is absent, i.e., $\delta_0 = 0$, the Hertzian interaction of the particle chain manifests its *essentially* nonlinear character. It is in that case that the speed of sound $c = (Ap\delta_0^{p-1})^{1/2}$ in the medium vanishes, the so-called sonic vacuum scenario. In this setting, highly nonlinear solitary waves, pioneered by Nesterenko [6, 10], have been identified and are the dominant energy carriers in the system [11].

Our principal question is thus formulated at the junction of these two important themes. On the one hand, for linear systems, acoustic wave propagation and the linear "phonon" spectrum are crucial for a fundamental understanding of propagating vs. evanescent waves in the system. On the other hand, no such entities arise in the sonic vacuum. In the latter case, highly localized (in fact, doubly exponentially localized [12]) solitary waves constitute the prototypical excitation of the system. Can then one seek spectral properties/spectral response in such highly nonlinear (finite lattice) settings and, if the answer is positive, how does such a response emerge? Surprisingly, in our system of choice (towards exploring these ideas), namely, the granular crystal, we computationally illustrate the existence of such a "nonlinear spectrum" as it arises in response to externally driving the system at different frequencies. The prin-

cipal mechanism for the emergence of this spectrum is the (nonlinearly induced) periodic and potentially quasi-periodic response of the system depending on the relative phases between the applied harmonic excitation on the one hand, and waves ("pulses") that appear to propagate in opposite directions, or to form standing wave patterns within the medium on the other. These inherently nonlinear notions have the potential to be widely applicable to systems without a linear spectrum, well beyond the specifics of our particular paradigm, and hence are of broad and diverse interest.

Only a few works have discussed the responses of granular crystals to harmonic excitation. In [13] nonlinear resonances in precompressed granular crystals were studied, together with certain bifurcations related with these motions; however, in distinction from the system considered in the present work, the systems in [13] possess a linear spectrum due to applied static precompression. In [14] the forced response of a two-bead granular crystal was considered and the pass and stop bands of this system were confirmed; given, however, the light damping of that system, no clear resonance peaks could be detected since the high-amplitude response became chaotic. To date the resonance and antiresonance structure of nonlinear sonic vacua have not been systematically studied; this is our aim here.

Setup. We consider a chain of beads interacting elastically via Hertzian contacts that are mathematically described (upon a suitable rescaling of amplitudes and of time [15]) as:

$$\begin{aligned}\ddot{x}_i &= (x_{i-1}-x_i)_+^{3/2} - (x_i - x_{i+1})_+^{3/2} \\ &\quad +\lambda\left[(\dot{x}_{i-1}-\dot{x}_i)H(x_{i-1}-x_i)\right. \\ &\quad \left. -(\dot{x}_i-\dot{x}_{i+1})H(x_i-x_{i+1})\right], \qquad (1)\end{aligned}$$

with $i = 1, \ldots, N$ with $N = 11$). The x_i's here represent the displacement of the particle centers from their equilibrium positions. The first two terms on the right hand side capture the bead-bead elastic interaction in our finite lattice, while the last two account for the linear dissipative dynamics, following the proposal of [16]. H denotes the Heaviside function, while $(\cdot)_+ = \max(\cdot, 0)$. These terms appear because of the tensionless character of the system, which implies there are no forces when beads are not in contact. The rescaling used to bring the system in the form (1) together with the numerical values of the system parameters are given in the Appendix.

The boundaries of the system under consideration consist of (a) an actuator exciting the (zero-th) bead with prescribed harmonic displacement at the left end and (b) an immobile wall on the right end. The latter is implemented as a fixed additional bead for which $x_{N+1} = \dot{x}_{N+1} = 0$, while the former is associated with $x_0 = A\sin(\omega t)$, i.e., a periodic excitation of a given frequency ω with an amplitude A. A schematic of the finite granular crystal is shown in Fig. 1. The result of this harmonic drive in the presence of *linear* coupling between adjacent nodes of a (finite) lattice would be to excite the

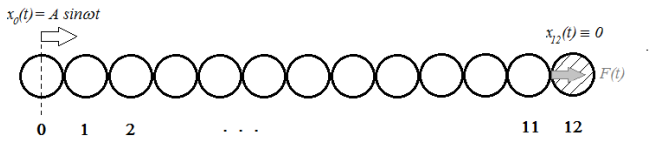

FIG. 1: (Color Online) A schematic of the finite granular crystal.

quantized (based on the boundary conditions) wavenumbers allowable by the lattice, and, accordingly, the frequencies corresponding to these wavenumbers based on the linear dispersion relation. In the present case, however, such a linear dispersion relation is *completely absent* (and so is a linear spectrum of frequencies) due to the essentially nonlinear character of the examined sonic vacuum. Accordingly, the resulting dynamics are expected to be completely tunable with the amplitude of the forcing, whereas the existence and structure of resonances in this system (i.e., of amplitude amplification on the granular chain at certain frequencies) is an interesting question. In the absence of linear (or linearized) dynamics, we now seek the corresponding response diagram in our highly nonlinear chain.

Results. The central result is summarized in Fig. 2. This represents the "nonlinear spectrum" of the system in response to its periodic actuation from the left boundary. To obtain this diagram, a combination of a fixed point algorithm (Newton's method for boundary value problems in time) and pseudoarclength continuation was used to numerically compute the branches of period-k solutions for various integers k. Similar to [17], this was accomplished by identifying fixed points of the stroboscopic map with a period of $k2\pi/\omega$ (i.e., k times the period of the applied harmonic excitation). The inset captures solely the *stable* (observable) response of the system, in the form of the maximal force exerted on the wall by the last bead over the period of the solution, plotted as a function of the drive frequency. It bears five clearly distinguishable peaks (which we will call "resonances" in the sense of local maxima of the response of the granular crystal), indicating that at these frequencies a maximal force is transmitted to the right end of the crystal. These peaks, as we will see in further detail below, correspond to solutions of different periods connected through the "backbone" presented in the inset. The diagram also features dips (which we will call "antiresonances") between the peaks, associated with frequencies that locally minimize the transmitted force. This resonance structure is clearly reminiscent of a linear spectrum, despite the fact that the basic ingredients of the latter are absent, such as the presence of a potential precompression force enabling the existence of a linearizable part in the corresponding dynamical equations. Moreover, the frequency range where these resonances and antiresonances occur lies within the nonlinear pass band of the chain [18], i.e.,

the frequency range where solitary pulses or spatially extended waves can propagate through the corresponding granular crystal of infinite extent, whereas for frequencies above 2 kHz, there is negligible force transmission. As we will see below, the *effective phase variation* (defined below and in the figure captions) between the applied excitation, and the nonlinear waves that result from it and travel along the chain, is crucial in the formation of these persistent resonance dynamics. We then delve into a more detailed exploration of these features.

We seek exact periodic orbits for the different frequencies within the range of our actuator (here, between 0 and 2.5 kHz). The resulting limit cycle solutions (given that this is a driven, damped system) are shown in the bifurcation diagram of the main part of Fig. 2. There, it can be discerned that there is a "backbone" of harmonic response (consisting of period-1 nonlinear solutions, with oscillation frequencies matching the driving frequency). In addition to identifying the existence of such a branch, we also explore its stability by means of Floquet analysis, identifying the corresponding Floquet multipliers of each point; see, e.g., [2, 17] for a detailed discussion. When these multipliers are within the unit circle, they correspond to stable dynamics, while their exiting the unit circle is associated with instability, which, in turn, is denoted by dashed lines in Fig. 2.

While the period-1 solution is stable at low and high frequencies, indicating a robust dynamical response of the system in these ranges, it undergoes a series of destabilizing bifurcations in intermediate frequency regimes, which lead to the observation of stable branches of higher period (subharmonic) solutions, i.e., of periodic responses with periods that are integer multiples of the period of the applied excitation. These subharmonics are denoted by different colors in Fig. 2. We note the existence of a resonant peak "within" each branch of periodic solutions, corresponding to a local maximum of the magnitude of the largest (over a single period of the solution) transmitted force to the right end of the chain. On the contrary, *antiresonances* corresponding to local minima of the largest transmitted force typically occur on stable parts of the period-1 solution branch. The detailed spatio-temporal nature of the periodic responses of the chain in resonances and antiresonances is of particular interest and will be discussed below. From Fig. 2 we deduce that the emergence of the period-2 solution occurs through a period-doubling bifurcation (and its disappearance through the "inverse" of the same bifurcation). However, the rest of the branches are isolated (so-called "isolas") and are not emerging directly from the primary 1:1 branch. It is also observed, however, that there are regions where we did not find low-period stable periodic solutions; in these regions (see the brown dash-dotted lines in Fig. 2), we expect the system response to be quasi-periodic (i.e., consisting of two harmonics with irrationally related frequencies) - or periodic with much higher integer periods, as these are known to arise in a systematic, interspersed pattern in quasiperiodic regimes [19–21].

Figure 3 depicts representative spatio-temporal variations of the kinetic energy in the regime of the 1:1 and 1:3 resonance peaks, together with the corresponding displacement waveforms for every bead during one period. Visual inspection of the kinetic energy space-time plots clearly suggests pulses traveling along the chain (part of the "nonlinear spectrum building blocks" mentioned in the abstract). These apparent waves are initiated on the left end of the chain, travel to the right, become (partially) reflected there, come back to the left end of the chain, and there interact again with the next "hit" of the actuator. The third component of each figure summarizes this pulse traveling in the form of an effective phase variation in the response of each bead: what is plotted is the time difference between the first occurrence during a period (at stationarity), of positive velocity for each bead, and for the leftmost bead of the chain; the almost perfect straight line plot clearly implies the traveling pulse nature of the long-term, stationary dynamics in the resonance peaks considered. This provides some insight into the nature of the relevant periodic, nonlinear solutions that dominate the response at resonance of the crystal lattice under the periodic external excitation.

In the parameter regime of the resonance peaks, it appears that the effective phase variation between the applied excitation and the traveling pulse initiated in the crystal is such that strong energy transfer from the exciting source occurs upon impact. This can be rationalized when we take into account that all resonances occur within the nonlinear pass band of the crystal, where traveling pulses constitute the nonlinear mechanism of energy transmission, and the applied excitation is in the form of a periodic train of impulses [6–9, 22]. In the case of 1:1 resonance (Fig. 3(a)) a strong impulse excitation occurs at precisely the time instant when the traveling pulse reflected from the right immovable boundary reaches the left end; one can deduce that the traveling pulses fully synchronize with the excitation source. At higher-order resonances, however, the time needed by the traveling pulse to fully traverse twice the length of the crystal is an integer multiple of the period of the applied pulses; for example in the 1:3 resonance peak (Fig. 3(b)) three periods of the excitation correspond to one period of the traveling pulse in the crystal; so the excitation inflicts a "strong impulse" at every third period (whereas secondary, weaker impulses also occur in between, but they are not strong enough to initiate new identifiable traveling pulses in the crystal). We conclude that the 1:n resonance peaks correspond to traveling pulses in the crystal with periods equaling n periods of the applied excitation. This is confirmed in the plots of the displacement waveforms of all beads during one full period (Fig. 3(c) and Fig. 3(d)). The traveling pulse character of these resonant responses of the crystal is also demonstrated in Fig. 3(e) and Fig. 3(f), where the effective phase variation (as defined above) of the individual bead responses is depicted as a function of space (more precisely, of bead

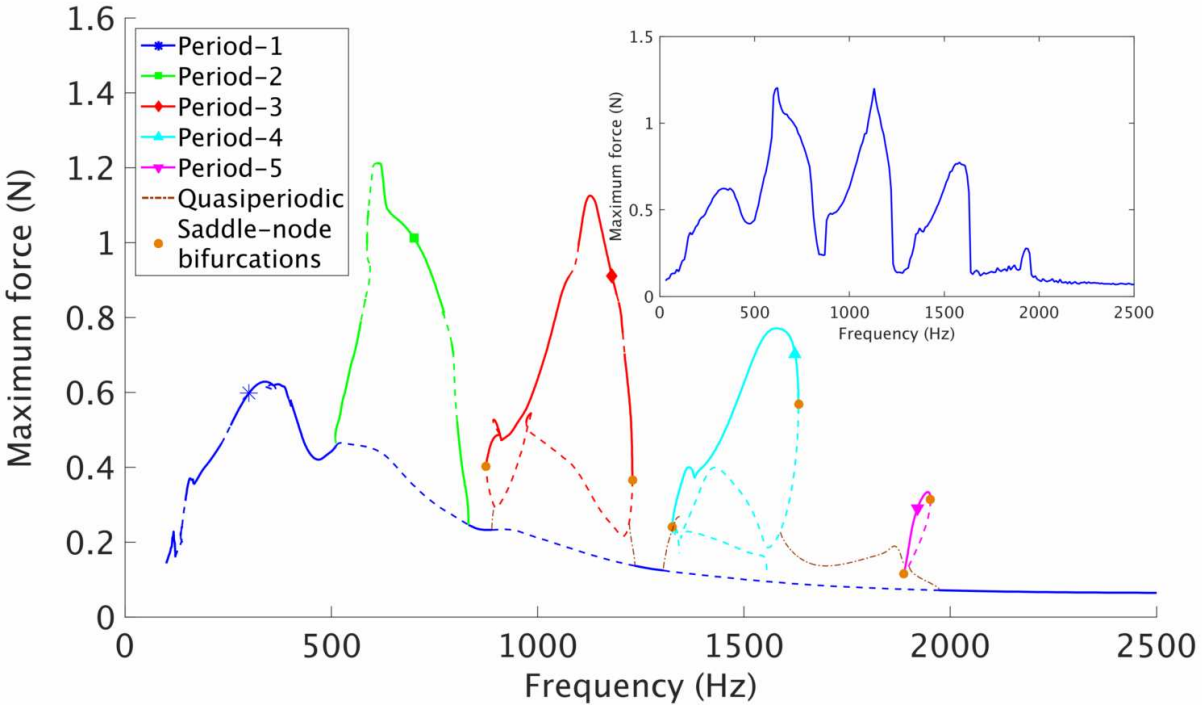

FIG. 2: (Color Online) Maximum force exerted on the fixed wall by the rightmost bead over one period of the periodic motion of the crystal. Branches corresponding to periods that are different integer multiples of the period of the actuator are shown in different colors. In the quasiperiodic case, the motion becomes dense on a T^2 torus, and the average force is estimated over a long time frame. The main graph showcases the different branches of nonlinear solutions (denoted by solid when stable, and dashed when unstable), while the inset incorporates solely the stable, observable response, i.e., the "nonlinear spectrum", that would be experimentally measured. Saddle-node bifurcations in which some of the higher period solutions terminate are also shown. The amplitude of the periodic excitation used here is 5×10^{-7} m.

number).

Having explored the resonances of our nonlinear spectral picture, let us now turn our attention to the corresponding *antiresonances*, corresponding to *local minima* of the (largest over one period) transmitted force to the right, immovable boundary. As mentioned previously all antiresonances are associated with stable 1:1 periodic responses, and this is confirmed by the results depicted in Fig. 4 where the second and third antiresonances are shown. What is interesting is that these minima of the largest transmitted force reside in the pass band of the crystal and alternate between resonances. This strongly suggests that the observation of antiresonances is not due to the incapacity of the granular crystal to transmit energy (in the form of traveling solitary pulses) but rather it is due to negative interference effects between left- and right-going traveling pulses; in such cases one might expect to observe apparent nonlinear *standing waves*. This is confirmed by the results of Fig. 4, where negative interference effects between apparent traveling pulses can be observed, giving rise to peculiar periodic responses. Indeed, it appears that there is a form of co-existence of traveling pulses (as in the resonance cases discussed previously) and apparent nonlinear standing waves in different parts of the crystal (traveling on the left side, standing on the right side, the side of the immovable wall). Such states of co-existence of different waveforms have been dubbed *chimeras* in other contexts; see [23] for a relevant discussion. This co-existence of apparently traveling and standing waves highlights the essentially nonlinear nature and the high complexity of the long-term, stationary response, and is corroborated by the results presented in Fig. 4(e) and Fig. 4(f). The negative interference of traveling pulses propagating in opposite directions in the crystal would explain the minimization of transmitted force in antiresonances, and the "low-intensity" impulses delivered by the exciting source in these cases. Such negative interference appears to lead to the formation of standing wave breathing patterns, such as the ones evident on the right side of the lattice in Fig. 4(e) and Fig. 4(f).

All of the above analysis has been performed for a fixed value of the forcing amplitude. However, our system permits exploration of a wide parameter space by means of the concurrent variation of both the forcing amplitude A and the forcing frequency ω. This more global perspective of the system is provided in Fig. 5. Here, we use the same color as before (in Fig. 2) to denote the bifurcation

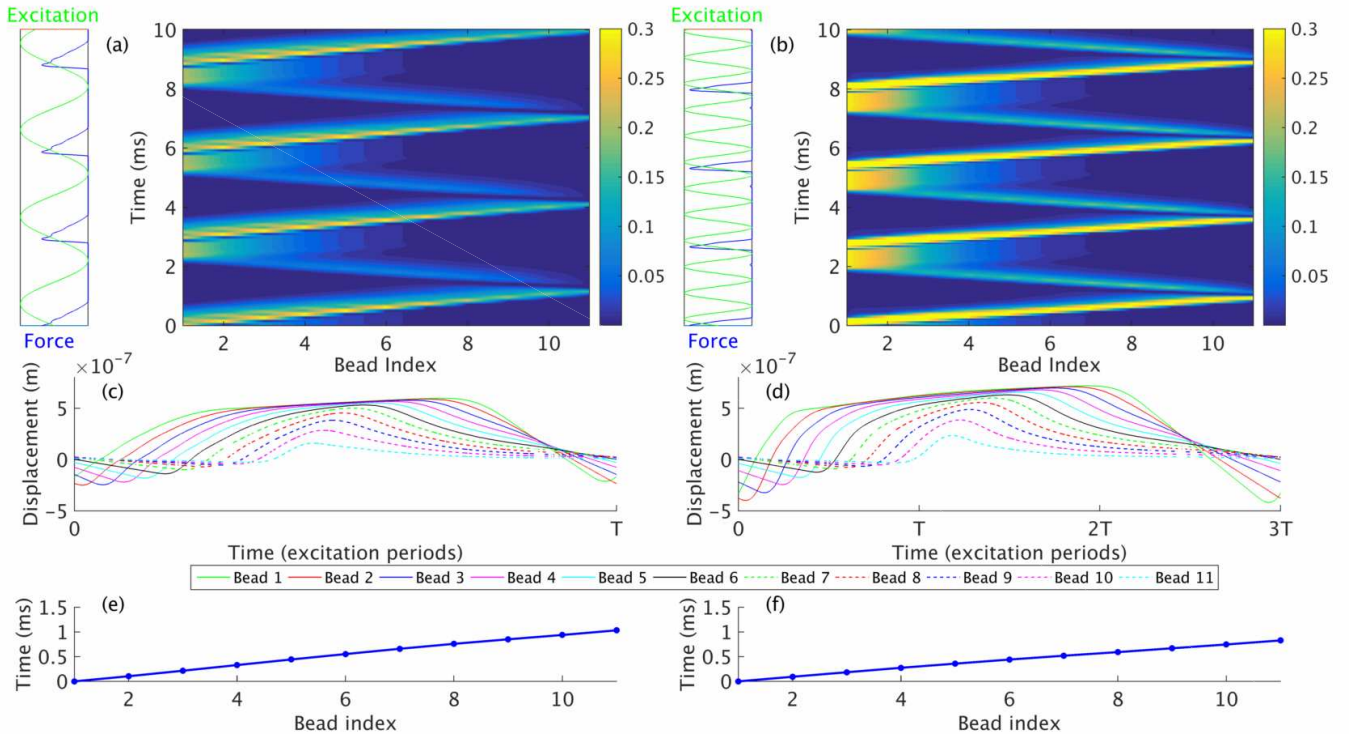

FIG. 3: (Color Online) (a),(b) Long-term, stationary spatio-temporal variation of the kinetic energy (scaled$\times 10^7$) for (a) 1:1 resonance (340 Hz) and (b) 1:3 resonance (1130 Hz); the input harmonic displacement and applied force excitations for each case are also shown on the left of each plot. While the crystal is composed of discrete units, we have used a smoothing color scheme in the figure to better underline the traveling/standing wave interpretation of the behavior. (c),(d) Displacement waveforms of every bead during one full period of the crystal motion. (e),(f) Effective phase variation of the individual bead responses (computed by the time instants when each bead's velocity first becomes positive and when the leftmost bead's velocity first becomes positive); this highlights the "traveling pulse" nature of the long-term, stationary dynamics of the granular chain at the resonance peaks.

loci of the different branches. For instance, the isolas of the period-4 and period-5 solutions terminate in pairs of saddle-node bifurcations (cf. Fig. 2) that are followed, in a two-parameter bifurcation diagram as the amplitude A varies, to produce resonance horns within which such solutions are contained in the (A, ω) space. We also highlight the locus of Neimark-Sacker period-1 bifurcations, giving rise to quasi-periodic solutions. The tips of these resonance horns lie, in fact, *on the Hopf (Neimark-Sacker) curve*, when the Floquet multipliers cross the unit circle at 4th and 5th roots of unity respectively. Needless to say that a host of other resonance horns (corresponding to every rational number) and many secondary bifurcations, both local and global, that cannot be feasibly computed, can also, in principle, be found in such a diagram (e.g. [19–21]). The bottom panels provide a sense of the variation of one of the system Poincaré sections (here, by monitoring the plane of the displacement and velocity of the 6th bead). The existence of a stable period-5 solution in both panels is illustrated by the green points; a coexisting unstable (saddle-type) period-5 is shown by the red points, while the unstable period-1 solution of the "backbone" branch is shown by the isolated point in the middle. The saddle- and node-period-5 solutions were initially born in a saddle-node on the torus; a remnant of this can be seen in that alternate sides of the unstable manifold of the saddles are attracted to different stable period-5 points. Global bifurcations, involving homoclinic manifold crossings and the associated horseshoe dynamics (see e.g. [24]), also occur within these resonance horns; while in the right panel a coexisting secondary stable quasiperiodic attractor emerges in the form of an invariant circle. In this last panel, one side of the saddle unstable manifolds is attracted by the stable period-5, while the other side is attracted by this torus; this change clearly suggests that a global bifurcation, namely a homoclinic interaction of the saddle invariant manifolds with each other, must occur along the path from point A to point B in parameter space. This is but a glimpse of the considerable complexity of this highly nonlinear system and the role of the nonlinear building blocks (stable and unstable periodic, as well as quasi-periodic solutions) naturally arising in the nonlinear analogue of the spectral picture we have outlined here.

Lastly, a natural question that can be raised concerns the role of the size of the chain in the results presented herein. Accordingly we have performed runs for a chain

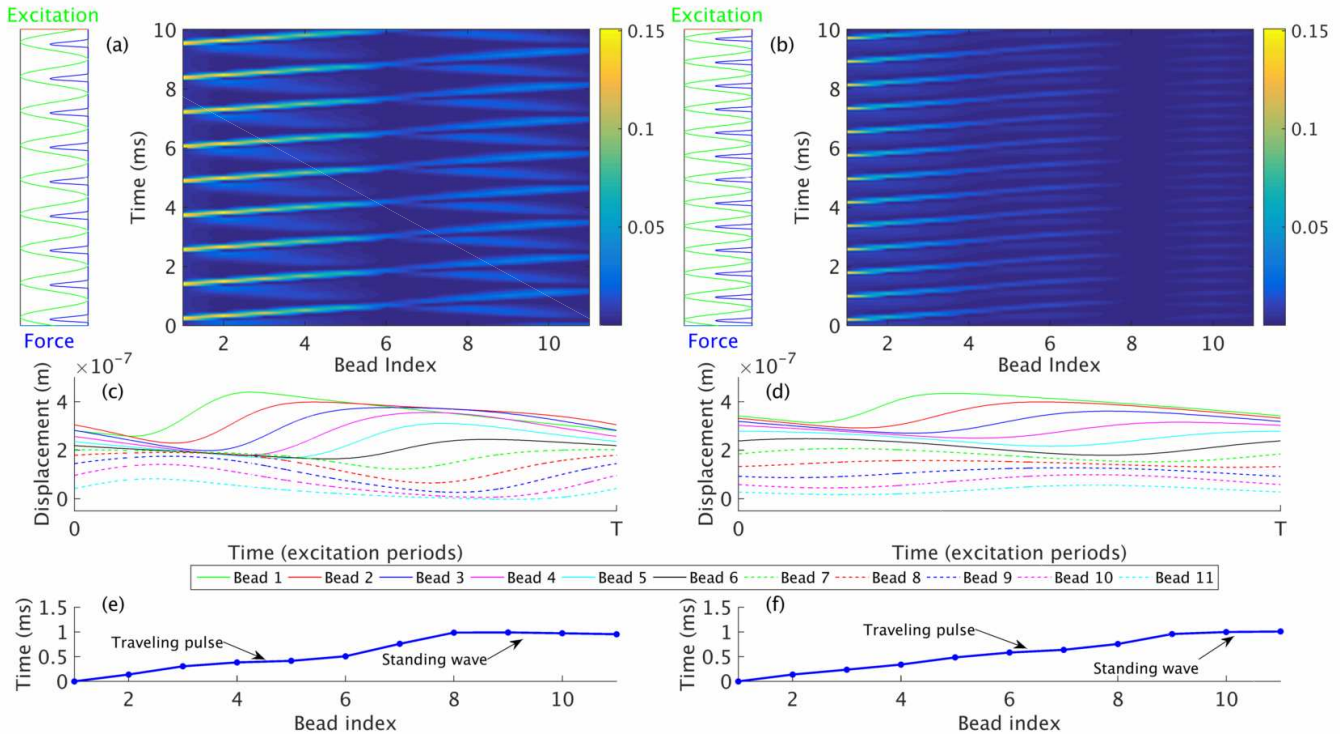

FIG. 4: (Color Online) (a),(b) Long-term, stationary spatio-temporal variation of the kinetic energy (scaled $\times 10^7$) for (a) the second antiresonance (860 Hz) and (b) the third antiresonance (1,260 Hz); the input harmonic displacement and applied force excitations for each case are also shown on the left of each plot. While the crystal is composed of discrete units, we have used a smoothing color scheme in the figure to better underline the traveling/standing wave interpretation of the behavior. (c),(d) Displacement waveforms of every bead during one full period of the crystal motion. (e),(f) Effective phase variation of the individual bead responses (computed by the time instants when each bead reaches maximum positive displacement and when the leftmost bead does); this highlights the chimera-like, partially "traveling pulse" and partially "standing wave" nature of the long-term, stationary dynamics of the granular chain at antiresonances.

of $N = 28$ beads. The results are shown in Fig. 6.

As we can see the principal peak structure remains the same, however the peaks have become narrower and two new visible peaks have appeared, corresponding to period-6 and period-7 solutions.

Conclusions and Future Challenges. In summary, in the present work, we focused on forced resonance spectra of highly nonlinear homogeneous granular crystals in the complete absence of linear acoustics (sonic vacua). Despite the lack of sound propagation, in the sense of classical acoustics, in the medium, we observed that a purely nonlinear analogue of the spectrum arises. This consists of harmonic and subharmonic responses to the external boundary drive of the granular crystal, leading to a series of peaks (resonances), reminiscent of the transmission frequency peaks in a finite, linearly coupled lattice. Here, the building blocks of the long-term, stationary responses are periodic and quasi-periodic orbits, whose existence and stability we explored computationally. Moreover, we illustrated how the periodic orbits corresponding to the energy transmission (resonant) peaks emerge out of periodic oscillations within the chain that can be attributed to highly nonlinear traveling pulses; the dips between them (antiresonances) are due to the emergence of a mix of apparent traveling pulses and standing waves, trapping the driver's energy in the vicinity of the lattice edges (a surface breathing mode, resembling a highly nonlinear analogue of the well-known Tamm states [25]). These results were extended into multiparametric variations (amplitude as well as frequency of the drive) and their generic nature was confirmed.

This proof-of-principle demonstration paves the way for systematic future investigations of such systems. On the one hand, it would be interesting and relevant to attempt to obtain a detailed experimental blueprint of the full nonlinear spectrum; indeed, experiments guided by these predictions and confirming their validity are underway, and will be reported elsewhere. On the other hand, numerous questions deserve further exploration, regarding the specifics of corresponding spectral pictures in systems with different types of nonlinear couplings, or in the presence of local nonlinearities as, e.g., in the cradle model of [26], as well as in the case of internal resonators [27]. A systematic understanding of the modifications of the spectral characteristics as N progressively increases would be another important aspect for future study. Extending these considerations to multidimensional systems with different geometric character-

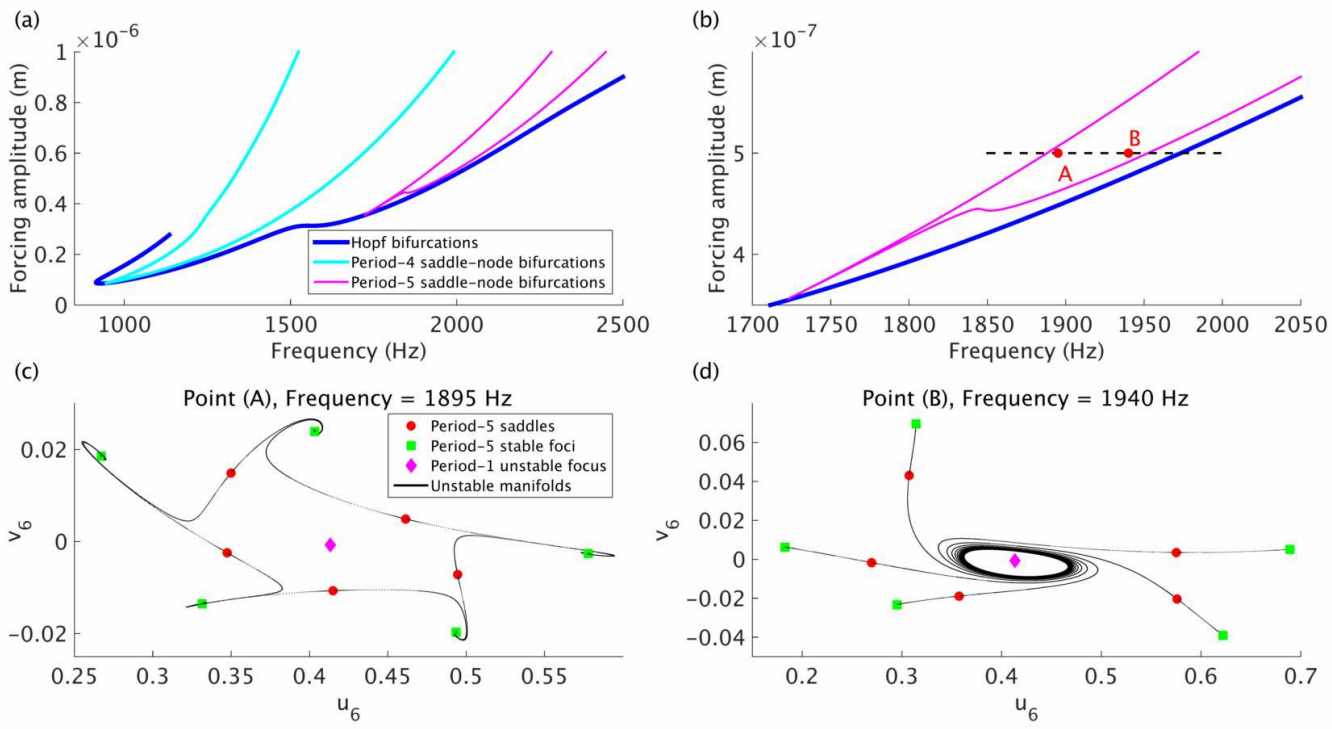

FIG. 5: (Color Online) (a) Partial two-parameter bifurcation diagram with respect to the forcing amplitude and the frequency of the actuator. The curves denote different bifurcations involving the nonlinear periodic solutions. More specifically: (1) the continuation of a Neimark-Sacker bifurcation of the period-1 solution (deep blue); and (2) continuation of saddle-node bifurcations of the period-4 and period-5 solutions (cyan and purple, respectively). The saddle-node bifurcations enclose two resonance horns that are born on the Neimark-Sacker curve when the Floquet multipliers cross the unit circle at the 4th and 5th roots of unity respectively. (b) Zoom-in of the period-5 resonance horn including a one-parameter cut across it. (c) Poincaré cut showing that the unstable manifolds of the saddles at point A above, along with the stable period-5 solutions, form a closed invariant set; at the horn boundary this was an invariant circle on which the saddles and the stable period-5s were "born" locked. The axes here are the dimensionless position and velocity of the 6th bead. (d) Moving towards point B in parameter space above, homoclinic crossings of the unstable and stable manifolds of the saddles have occurred and two attractors now coexist, a stable invariant circle (a quasi-periodic solution) and a stable node period-5 solution.

istics [28, 29] would also represent a significant generalization of the present work. Such studies are presently in progress and will be reported in future publications.

Acknowledgments. AFV would like to acknowledge the support of MURI grant US ARO W911NF-09-1-0436. Dr. David Stepp is the grant monitor. DP, MOW, PGK and IGK gratefully acknowledge the support of US AFOSR through grant FA9550-12-1-0332. PGK's work at Los Alamos is supported in part by the US Department of Energy.

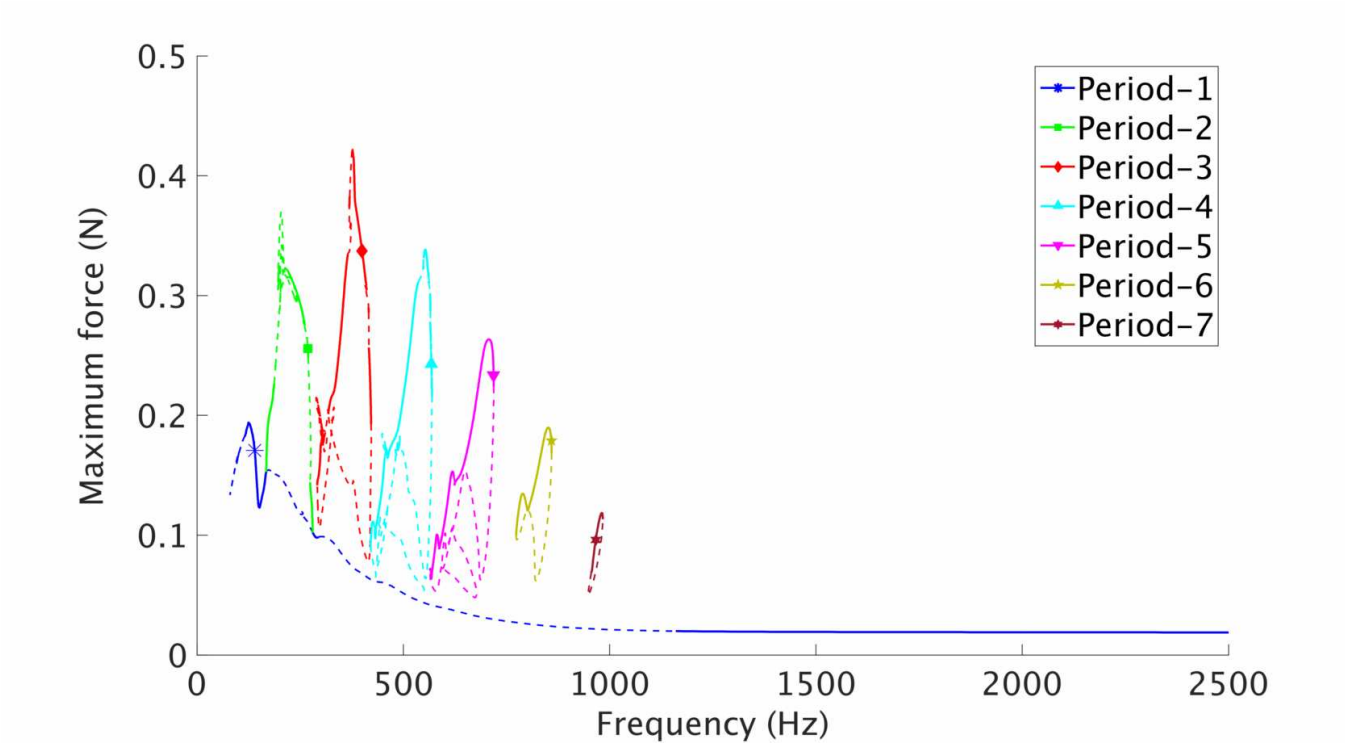

FIG. 6: (Color Online) Maximum force exerted on the fixed wall by the rightmost bead over one period of the periodic motion of the crystal. Case of $N = 28$ beads. The principal peak structure remains the same, however the peaks have become narrower and two new visible peaks have appeared, corresponding to period-6 and period-7 solutions.

[1] L. Brillouin, Wave Propagation in Periodic Structures, Dover (New York, 2003).
[2] S. Flach and C. R. Willis, Phys. Rep. **295**, 181 (1998); S. Flach, A.V. Gorbach, Phys. Rep. **467**, 1 (2008).
[3] E. Ben-Naim, P.L. Krapivsky, J. Phys. A **45**, 455003 (2012).
[4] P. Rosenau and J. M. Hyman, Phys. Rev. Lett. **70**, 564 (1993); P. Rosenau, Phys. Rev. Lett. **73**, 1737 (1994); P. Rosenau, J.M. Hyman, and M. Staley, Phys. Rev. Lett. **98**, 024101 (2007).
[5] B. Dey, M. Eleftheriou, S. Flach, and G. P. Tsironis, Phys. Rev. E **65**, 017601 (2001).
[6] V.F. Nesterenko, Dynamics of Heterogeneous Materials, Chapter 1, Springer-Verlag (New York, 2001).
[7] S. Sen, J. Hong, J. Bang, E. Avalosa, R. Doney, Physics Reports **462**, 21-66 (2008).
[8] P.G. Kevrekidis, IMA J. Appl. Math. **76**, 389 (2011).
[9] G. Theocharis, N. Boechler, and C. Daraio, in *Phononic Crystals and Metamaterials*, Ch. 6, Springer Verlag, (New York, 2013).
[10] V. F. Nesterenko, J. Appl. Mech. Tech. Phys. **24**, 733 (1983).
[11] E. J. Hinch and S. Saint-Jean, Proc. R. Soc. London, Ser. A **455**, 3201 (1999).
[12] A. Chatterjee, Phys. Rev. E **59**, 5912 (1999); J.M. English and R.L. Pego, Proc. Amer. Math. Soc. **133**, 1763 (2005); K. Ahnert and A. Pikovsky, Phys. Rev. E **79**, 026209 (2009).
[13] J. Lydon, G. Theocharis, C. Daraio, Phys. Rev. E **91**, 023208 (2015).
[14] J. Lydon, K.R. Jayaprakash, D. Ngo, Y. Starosvetsky, A.F. Vakakis, C. Daraio, Phys. Rev. E **88**, 012206 (2013).
[15] K. R. Jayaprakash, Y. Starosvetsky, and A.F. Vakakis, Phys. Rev. E **83**, 036606 (2011).
[16] A. Rosas, A.H. Romero, V.F. Nesterenko, and K. Lindenberg, Phys. Rev. Lett. **98**, 164301 (2007).
[17] C. Chong, F. Li, J. Yang, M.O. Williams, I.G. Kevrekidis, P.G. Kevrekidis, C. Daraio, Phys. Rev. E **89**, 032924 (2014).
[18] K.R. Jayaprakash, Y. Starosvetsky, A.F. Vakakis, M. Peeters, G. Kerschen, Nonlinear Dynamics **63**, 359-385 (2011).
[19] D. G. Aronson, M. A. Chory, G. R. Hall, R. P. McGehee, Comm. in Math. Phys. **83**, 303-354 (1982).
[20] I.G. Kevrekidis, L.D. Schmidt, R. Aris, Chem. Eng. Sci. **41**, 1263-1276 (1986).
[21] D. G. Aronson, R. P. McGehee, I. G. Kevrekidis, and R. Aris, Phys. Rev. A **33**, 2190-2192 (1986).
[22] M.A. Hasan, S. Cho, K. Remick, A.F. Vakakis, D.M. McFarland, W.M. Kriven, Granular Matter **17**, 49 (2015).
[23] D.M. Abrams and S.H. Strogatz, Phys. Rev. Lett. **93**, 174102 (2004).
[24] J. Guckenheimer, P. Holmes, Nonlinear Oscillations, Dynamical Systems, and Bifurcations of Vector Fields, Springer (New York, 1983).
[25] See e.g. Yu.S. Kivshar and M.I. Molina, Wave Motion **45**, 59 (2007).
[26] G. James, Models Meth. Appl. Sci. **21**, 2335 (2011); G. James, P.G. Kevrekidis, J. Cuevas, Physica D **251**, 39 (2013).
[27] L. Bonanomi, G. Theocharis, C. Daraio, Phys. Rev. E **91**, 033208 (2015); G. Gantzounis, M. Serra-Garcia, K. Homma, J.M. Mendoza, C. Daraio, J. Appl. Phys. **114**, 093514 (2013); E. Kim, F. Li, C. Chong, G. Theocharis, J. Yang, and P.G. Kevrekidis, Phys. Rev. Lett. **114**, 118002 (2015).
[28] I. Szelengowicz, M. A. Hasan, Y. Starosvetsky, A. Vakakis, and C. Daraio, Phys. Rev. E **87**, 032204 (2013).
[29] A. Leonard, C. Daraio, Phys. Rev. Lett. **108**, 214301 (2012); A. Leonard, C. Chong, P.G. Kevrekidis, C. Daraio, Granular Matter **16**, 531 (2014).

Appendix. We consider a one-dimensional chain of spherical elastic beads in Hertzian contact with no precompression:

$$
\begin{aligned}
m\frac{d^2u_1}{dt^2} &= \frac{4}{3}E^*\sqrt{\frac{R}{2}}\left[(A'\sin(2\pi ft)-u_1)_+^{3/2}-(u_1-u_2)_+^{3/2}\right] \\
&\quad +D\left[(2\pi fA'\cos(2\pi ft)-\dot{u}_1)H(A'\sin(2\pi ft)-u_1)-(\dot{u}_1-\dot{u}_2)H(u_1-u_2)\right], \\
m\frac{d^2u_i}{dt^2} &= \frac{4}{3}E^*\sqrt{\frac{R}{2}}\left[(u_{i-1}-u_i)_+^{3/2}-(u_i-u_{i+1})_+^{3/2}\right] \\
&\quad +D\left[(\dot{u}_{i-1}-\dot{u}_i)H(u_{i-1}-u_i)-(\dot{u}_i-\dot{u}_{i+1})H(u_i-u_{i+1})\right], \\
m\frac{d^2u_N}{dt^2} &= \frac{4}{3}E^*\sqrt{\frac{R}{2}}\left[(u_{N-1}-u_N)_+^{3/2}-(u_N)_+^{3/2}\right] \\
&\quad +D\left[(\dot{u}_{N-1}-\dot{u}_N)H(u_{N-1}-u_N)-(\dot{u}_N)H(u_N)\right],
\end{aligned}
$$

where

m – mass of each bead (28.84 g),
R – radius of each bead (9.525 mm),
A' – amplitude of the actuator (5×10^{-7} m),
f – frequency of the actuator ,
D – viscous damping coefficient

between beads (100 Ns/m),

$$E^* = \frac{E}{2(1-\nu^2)},$$

E – Young's modulus (193 GPa),

ν – Poisson's ratio (0.3).

Define

$$\begin{aligned} A_0 &= A' \text{ (original amplitude of the actuator)}, \\ x_i &= \frac{u_i}{A_0}, \\ A &= \frac{A'}{A_0}, \\ \bar{t} &= \tau t, \\ \lambda &= \frac{D}{m\tau}, \text{ and} \\ \omega &= 2\pi f, \end{aligned}$$

where

$$\tau = \sqrt{\frac{4E^*\sqrt{\frac{R}{2}A_0}}{3m}}.$$

Using the variables defined above we end up with our nondimensionalized system of equations

$$\begin{aligned} \ddot{x}_i = {} & (x_{i-1} - x_i)_+^{3/2} - (x_i - x_{i+1})_+^{3/2} \\ & + \lambda \left[(\dot{x}_{i-1} - \dot{x}_i) H(x_{i-1} - x_i) \right. \\ & \left. - (\dot{x}_i - \dot{x}_{i+1}) H(x_i - x_{i+1}) \right], \end{aligned} \tag{1}$$

with $x_{N+1} = \dot{x}_{N+1} = 0$ and $x_0 = A\sin(\omega t)$.